

Effects of Diffusion Weighted Image Interpolation for Motion and Distortion Correction on Tensor Statistics

Mustafa Okan Irfanoglu^{1,2}, Lindsay Walker^{1,2}, Raghu Machiraju³, and Carlo Pierpaoli¹

¹NIH, NICHD, Bethesda, MD, United States, ²Center for Neuroscience and Regenerative Medicine, Uniformed Services University of the Health Sciences, Bethesda, MD, United States, ³Computer Sciences & Engineering, The Ohio State University, Columbus, OH, United States

Introduction: Processing of clinical diffusion weighted images (DWIs) for diffusion tensor imaging (DTI) applications requires correction for motion, eddy current distortions [1], and susceptibility induced EPI distortions [2]. These corrections can be obtained by image registration techniques performing interpolation on the original images [1,3,4]. The effects of the interpolation strategies involved in these registrations, on tensor derived quantities, have mostly been disregarded in the community; however, the outcomes of a DTI study can significantly vary based on the employed interpolation scheme, especially for approaches that employ whole-brain histograms. In this work, we analyze the effects of three of the most commonly used interpolation methods on tensor derived quantities.

Materials & Methods:

Data: The effects of interpolation were demonstrated on two datasets. One healthy subject was scanned with a 3.0T GE Excite scanner using an eight channel coil. DWI datasets were acquired with FOV= 24×24 cm, slice thickness= 2.5 mm, matrix size= 128×128, 66 axial slices. The diffusion data consisted of ten images with $b=0$ s/mm², ten images with $b=300$ s/mm² and 60 images with $b=1100$ s/mm². In addition to the real subject data, a synthetic, analytical phantom was created to quantitatively assess interpolation performance and the amount of artifacts. The phantom was generated from several spatially continuous analytical functions for the diffusion tensors, which divided the image space into four regions with different diffusion properties to emulate real data (matrix size 128x128x64). The diffusion weighted images were then obtained for a given SNR using the same experimental design of the subject data.

DTI Processing: The diffusion weighted images of the subject data were first corrected for motion and eddy-current distortions. Subsequently an additional EPI distortion correction step was performed by elastically registering the first $b=0$ s/mm² to its corresponding undistorted structural image with B-Splines transformation of grid size 7x7x7. The computed deformation was applied to all DWIs belonging to the DWI dataset. Finally, all the DWIs were transformed onto the structural image's space yielding four consecutive transformation applications, which were then combined into a single deformation field \mathcal{D}_f . For the synthetic data, the inverse of this deformation field, \mathcal{D}_f^{-1} , was used to analytically generate the distorted phantom data without any interpolation. Subsequently, \mathcal{D}_f was applied to generate corrected data with interpolation. For each data, the diffusion tensors were computed from the interpolated images using non-linear regression.

Analysis Framework: Three interpolants were used for analysis: Nearest neighbor (NN), trilinear and cubic. Even with the same deformation field \mathcal{D}_f , these interpolants yield different final diffusion weighted images due to their different methods in estimating the "continuous" images. For the subject data, the whole-brain distributions of fractional anisotropy (FA) and trace of the diffusion tensor (Trace(D)) maps were compared for each interpolation method. Additionally, tissue interfaces were determined using a segmentation approach and the same distributions were computed within a neighborhood of these interfaces to observe the changes of partially affected voxels. For the synthetic data, the differences in FA, Trace(D) and primary directions between the interpolated image and the ground truth were computed. These differences were summed up along two image axes and plotted against the other.

Results: Figure 1 displays the FA and Trace(D) maps of the same subject obtained with the three interpolation techniques. The NN data suffers, as predicted, from discontinuities in CSF regions (Trace(D)) and the body of corpus callosum (FA). In the trilinear case, the FA in the body of CC is significantly higher than that of the cubic case. On the contrary, the FA in the subcortical white matter regions in the cubic data is higher than the corresponding regions in the trilinear case. Figure 2 displays a whole brain histogram and a histogram of partially contaminated voxels of the FA image. In both cases, the histograms differ significantly. For the whole brain, the NN interpolation yields the highest frequencies at higher FA values, but the other kernels have these probabilities decreased due to their smoothing effects. Figure 3 displays a slice from our analytically continuous synthetic data after having undergone the two transformations. Figure 4 displays the differences in FA between the interpolated data and the ground truth. The cubic interpolant yields the lowest errors while the errors of NN and trilinear interpolants are similar. The errors are larger at region interfaces and tend to decrease at the center of homogeneous regions.

Discussions: Even though their effects are generally disregarded in the diffusion community, the interpolation strategies involved during DWI processing can significantly alter diffusion based analysis outcomes. This behavior would be magnified for histogram based analysis such as normal appearing white matter versus healthy white matter comparisons, hence can lead the researchers to draw inaccurate conclusions. The NN interpolant produces images with discrete features, hence is not suitable for most situations. Cubic interpolant yields the most accurate results but an interpolation scheme specialized for diffusion imaging data is still needed.

References: 1. Rohde G et al., TBE, 2005;. 2. Jezzard P. et al., Magn Reson Med ,1995;. 3. Wu M. et al., ISMRM, 2007. 4. Kybic et al., TMI, 2000.

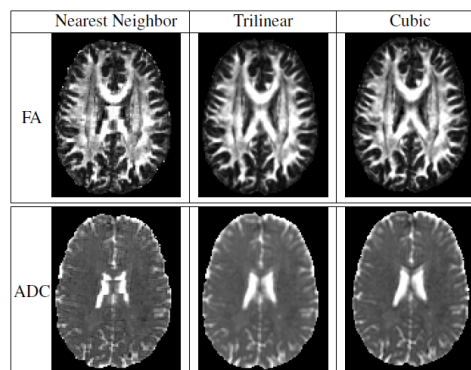


Figure 1. FA and ADC maps with three different interpolation techniques from data of the same subject.

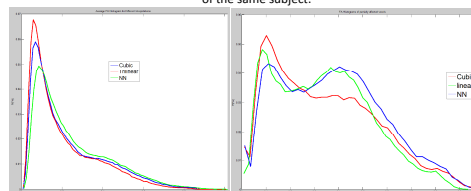


Figure 2. Left: Whole brain FA histogram with the 3 interpolants. Right: FA histogram from partially contaminated voxels.

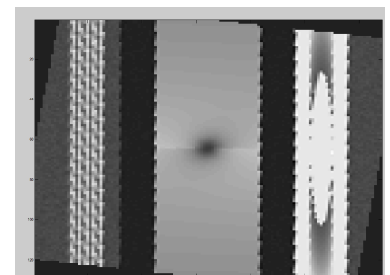


Figure 3. Synthetic data transformed once analytically and transformed back with interpolation.

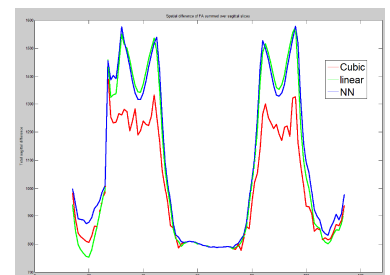


Figure 4. Difference between the ground truth FA and the interpolated version.